Obtaining C_2 and C_3 Products from Methane Using Pd/C as Anode in a Solid Fuel Cell-type Electrolyte Reactor

Andrezza S. Ramos,[a] Monique Carolina L. Santos,[a] Camila M. Godoi,[a] Almir Oliveira Neto,[a] and Rodrigo Fernando B. De Souza*[a]

Methane was converted into C2 and C3 products under mild conditions using a single stage solid electrolyte reactor, using a proton exchange membrane fuel cell as a SER-FC and Pd/C as an electrocatalyst prepared by the reduction method of sodium borohydride. This electrocatalyst has a cubic pattern of palladium centered on the face and an average size of nanoparticles close to 6.4 nm, according to the literature. Differential mass spectrometry reveals the chemical profile of species obtained from the oxidation of methane with ionic currents (Ii) at m/z = 16, 28, 30, 32, 44, 46 and 60. In many cases, Ii can be assigned to more than one species; therefore, complementary ATR-FTIR experiments were performed. The ATR-FTIR spectra confirmed the presence of C2 and C3 compounds such as ethane, ethanol, acetaldehyde, acetic acid and propane. Considering the low amount of water in the reaction medium, these results may be associated with the use of Pd/C electrocatalysts responsible for the activation of the water molecule.

The availability of natural gas currently rivals with oil; however, this hydrocarbon is not as versatile as crude oil.[1] The main component of natural gas is methane, the most stable hydrocarbon, with the very high dissociation energy of C–H bond (435 kJ mol^{-1}).[2] Its tetrahedral structure is difficult to polarize; therefore, it makes this molecule almost inert to mild conditions.[3] Turning this gas into higher value-added products is a great goal.

Current approaches to utilization of methane involve mainly high-temperature processes to produce syngas ($H_2 + CO$), which further can be transformed into methanol or fuels.[2] The ethane is a vital building block in the chemical industry with an expectedly of increasing demand in obtaining C2 or longer compounds.[4] The oxidative coupling of methane (OCM) is a direct and exothermic process and not limited by any thermodynamic constraints.[1a]

The key of OCM reaction is the formation of methyl radicals. This radical, in the gas phase, reacts with methane to form ethane and other products.[1b,5] However, the OCM reaction is fulfilled at high temperature (above 600°–800 °C); a condition that allows methane combustion and the reaction that competes with the generation of CO and H_2 to occur.[6] Otherwise, similar to what happens on OCM reaction in high temperature, the methane can be activated at mild condition when the water activation generates "reactive oxygenated species" (ROS) as a $HO^{\bullet}$ species. This radical causes the methane C–H bond scission leading to the reactive methyl radical formation, which in turn reacts with water molecules to produce methanol and hydrogen.[7] These routes occur by like Fenton-reaction,[7a] or photo catalysis[8] and electrocatalysis.[9] As cited, the methyl radical that reacts with water molecules does not produce more complex species than methanol and its oxidation products. Due to most photochemical and electrochemical processes occur in aqueous medium, products with C2 or C3 are rarely observed.

The electrochemical reactors like solid electrolyte reactors – fuel cell type (SER-FC) are basically composed by two electrodes separated by an ion-conducting polymer that can operate in continuous flow; due to the solid electrolyte, the amount of water present in the reactional medium is drastically lower than electrochemical cell medium.[10] Proton exchange membrane fuel cell (PEMFC) was initially built to operate with H_2 and O_2;[11] this device allows that the formed radicals have higher chances to collide with other molecules containing carbon in the aqueous medium and, thereby, to occur their carbon chain growth.

In the last years, some authors have studied the application fuel cells at low temperatures for partial oxidation of methane at mild conditions;[12] the most bountiful products were the methanol or formate species, additionally other products such as isopropanol and acetaldehyde are reported with less frequency.[12b] However, there are still little accumulated data on the subject, as a novel electrocatalysts and material flux.[9b]

The palladium is still frequently employed as anodic electrode for the activation of small organic molecules in PEMFC.[12c,13] Winiwarter et al.[13a] showed that Pd could be promising for the application in this reactor type, because for this metal (M) there is formation of a thin layer of PdO (M–O) on electrocatalyst surface, where the oxide can activate the C–H bond in methane[14] and the water molecule;[15] it is also utilized for hydrocarbon oxidation,[16] due to its carbophilic properties. In this work, the application of solid electrolyte reactors (SER) PEMFC-type in mild conditions was studied to

[a] Dr. A. S. Ramos, M. C. L. Santos, C. M. Godoi, Dr. A. Oliveira Neto, Dr. R. Fernando B. De Souza
Centro de Celula a Combustivel e Hidrogenio
Instituto de Pesquisas Energéticas e Nucleares, IPEN/CNEN-SP
Av. Prof. Lineu Prestes, 2242 Cidade Universitária, CEP 05508–000, São Paulo, SP (Brazil)
E-mail: aolivei@ipen.br

Supporting information for this article is available on the WWW under https://doi.org/10.1002/cctc.202000297

promote partial oxidation of methane on Pd/C and to verify the occurrence of oxidative coupling of this hydrocarbon.

The physical characterization of Pd/C electrocatalyst is illustrated in Figure 1. It is possible to see the peaks about 2θ ≈40°, 47°, 68°, 82° and 87° associated, respectively, to (111), (200), (220), (311) and (222) planes of face-centered cubic (fcc) structure, in accord to Pd (JCPDF #89-4897) (Figure 1a). TEM micrograph image (Fig1b) shows the good dispersion on the nanoparticles support, and particle diameter; electrocatalysts present sizes for at 6.5 nm (Figure 1c) in agreement with the literature.[12c,16a,17]

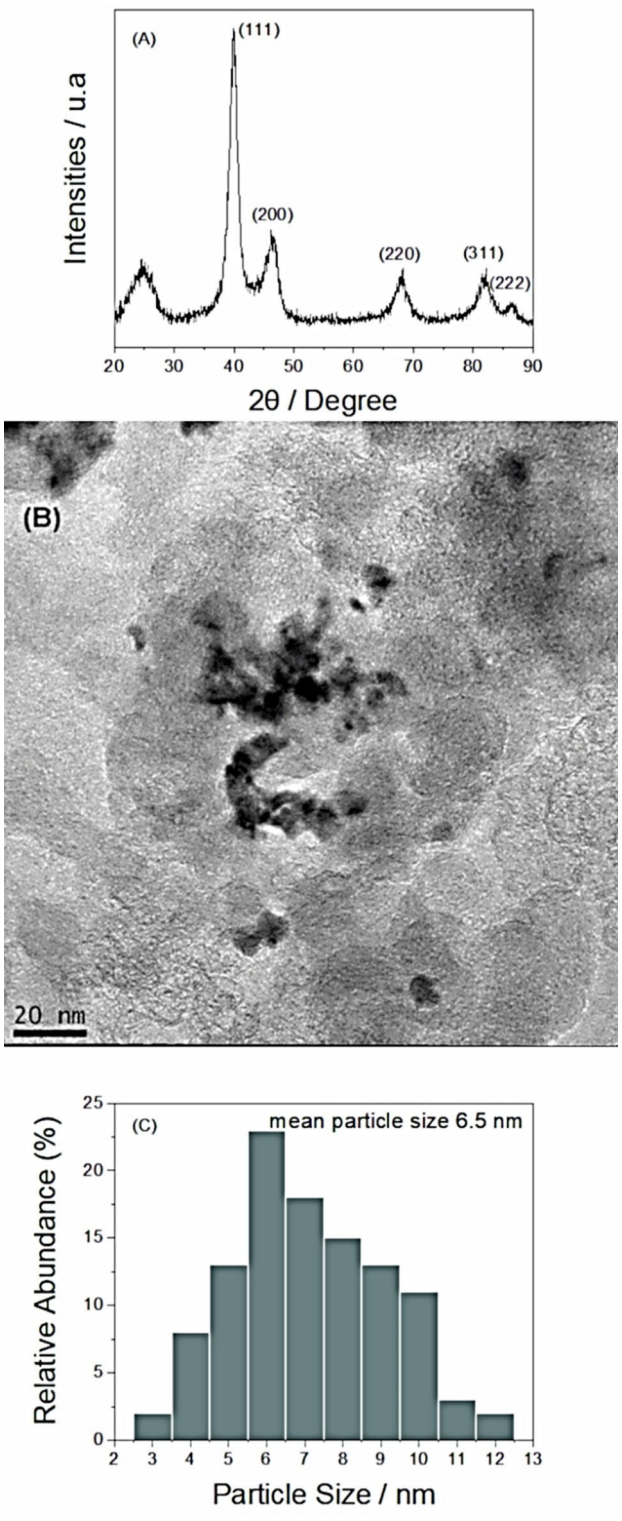

Figure 1. (a) X-ray diffractograms, (b) TEM micrograph, (c) histogram of the particle size distribution of the Pd/C catalysts prepared by $NaBH_4$ reduction process.

Figure 2 presents the j/V curve SER-FC during methane oxidation in the anodic chamber with a feed mixture of methane (room temperature) and H_2O vapor (85 °C) catalyzed by Pd/C. The Open Circuit Voltage (OCV) for this device measured is about −0.2 V and the current is increasing nonlinear form with the potential increasing. It means that there is more than one process in the same potential range about −0.2 until 0.8 V. After 0.3 V the current increases, indicating the reduction in the charge transfer resistance, similar to values observed by Lee.[12a]

SER-FC effluent was online with Differential Mass Spectroscopy (DMS) at constant flow rate. The chemical species obtained from partial oxidation of methane showed m/z at 16, 28, 30, 32, 44, 46, and 60. In Figure 3 are presented the ion current (I_i) for all species, except m/z = 28 that does not present an appreciable variation. Decrease of I_i to m/z = 16 attributed to methane, with increasing the potential. This would be consistent in the case of consumption of methane during the reaction and this behavior is linked to the appearance of I_i for other possible compounds that are formed. The methane concentration was decreased with the increase in potential, similar to reported by Lee et al..[12a] The signal for m/z = 30 presents two peaks near −0.1 V and 0.2 V, with a valley between these two maxima, may be the sum of the I_i corresponding to formaldehyde and/or ethane, isomers compounds. To the signal at m/z = 32, assigned to methanol, it is observed a current increment in the range of −0.2 V to −0.1 V. Between −0.1 V to 0 V, the I_i strongly decreases, and from this potential, it has a less intense description. This rapid decrease may be linked to the consumption of alcohol produced in the SER-FC, for an electric current generation, as reported by Nandenha[18] and Santos[12c] in this potential range.

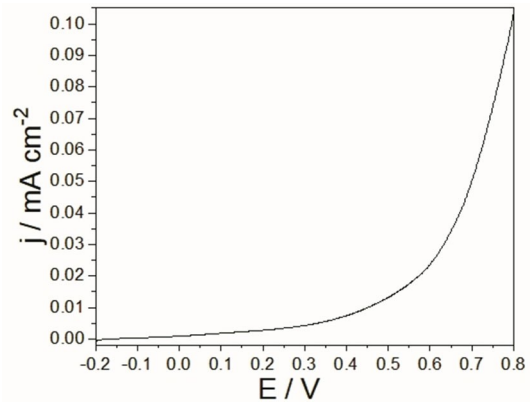

Figure 2. j/V curve of electrochemical methane oxidation over a Pd/C anode at room temperature in a SER-FC with v = 1 mV s^{-1}.

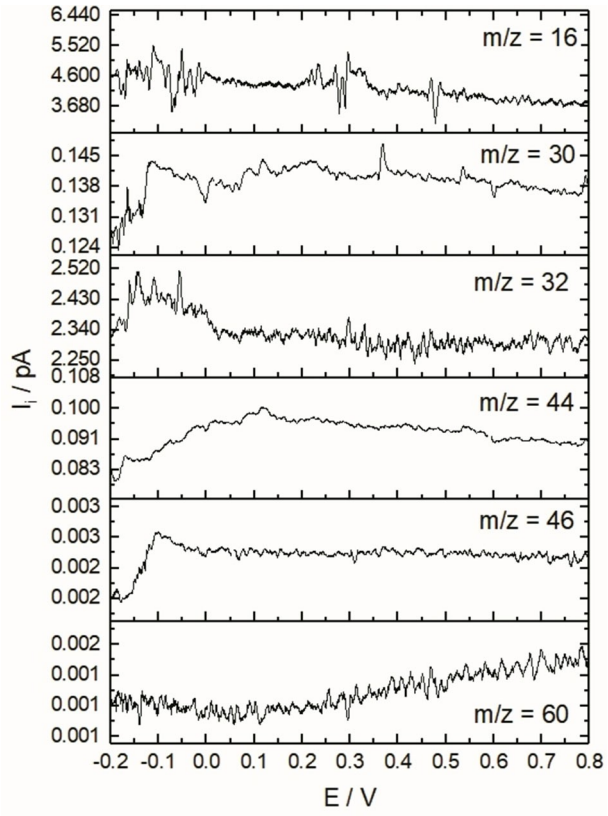

Figure 3. Mass spectroscopy profile versus potential values of the products obtained from methane oxidation on Pd/C anode of SER-FC.

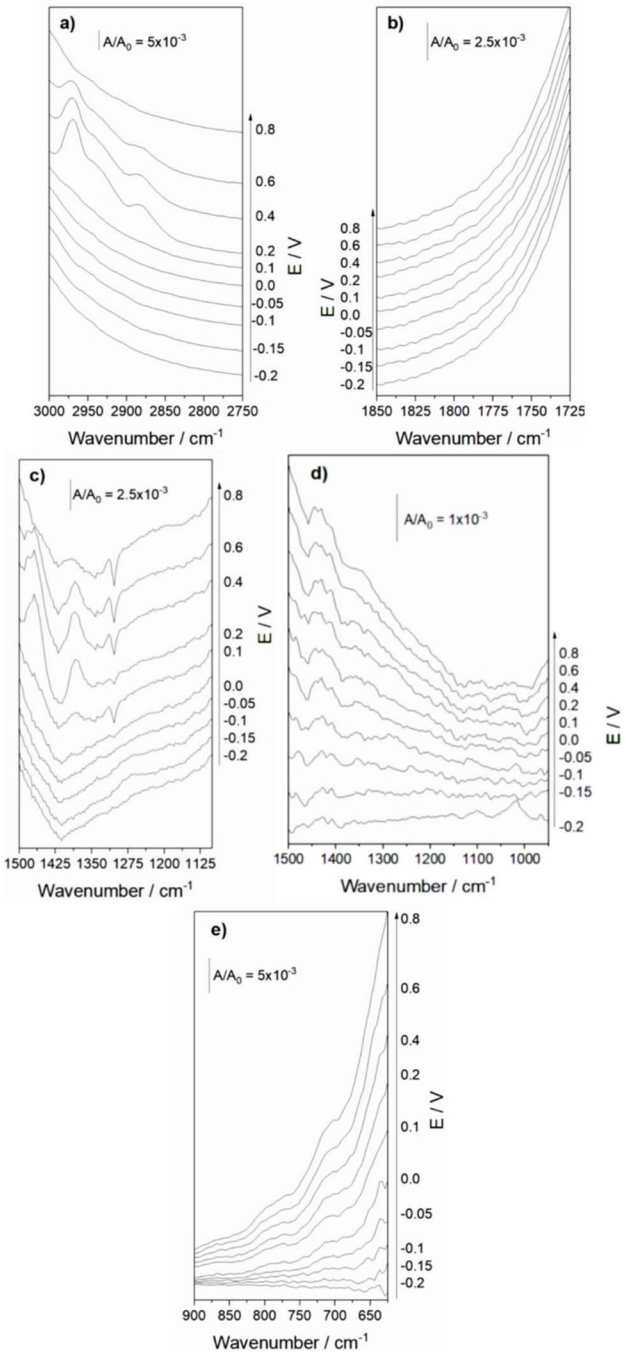

Figure 4. ATR-FTIR spectra of the products obtained in various potentials of SER-FC effluent collected in hexane a), b), c) and water d), e).

The CO_2, acetaldehyde and propane are also possible products and would have signal with m/z = 44. For this I_i we see an increase from −0.20 V to 0.15 V. There is a decrease until 0.6 V, when the measured current is reduced abruptly and remains almost constant up to 0.8 V, indicating lower production or even consumption of the corresponding species. At m/z = 46, which can be attributed to ethanol and formic acid, the I_i increase from −0.15 V to −0.1 V, followed by a decreasing behavior to −0.05 V and proceeds almost stable to 0.8 V. Formic acid may also be an oxidizing product of methanol, due the signal appears 50 mV more positive than methanol onset signal and declines with the decrease of signal m/z = 32 (methanol). The signal at m/z = 60 corresponding to as well to acetic acid as methylformate, becomes more apparent when I_i decreases from −0.2 V to 0.1 V. Due to the formation of ester by the abundance of species with C1, in this condition, the population of m/z = 60 decreases after 0.15 V.

The DMS shows the profile of the appearance of species from partial methane oxidation and possible OCM; however, in many cases the I_i can associate with more than one chemical specie. Therefore, SER-FC effluent samples were also analyzed by infrared spectroscopy to confirm the chemical species obtained, for even though, their intensities are not comparable. Figure 4 illustrates the ATR-FTIR spectra in the aqueous and hexane fractions of the samples taken from the effluent reactor. It is possible to observe the characteristic bands of each species in function of potential.

Bands in aqueous sample are observed at 1482 cm^{-1} for CH_3 d-deform,[19] 1082 cm^{-1} and 1030 cm^{-1} (Figure 4d) commonly attributed to methanol[12c,18] showed a pattern similar to I_i at m/z = 32. The signal m/z = 30 was attributed to two species: i) formaldehyde, commonly reported in partial methane oxidation at mild conditions.[12a,18,20] Its evolution can be observed by the 1249 cm^{-1} band (Figure 4d) CH_2 rock of formaldehyde[21] that

behaves crescent from −0.2 V to −0.05 V and then, disappears. In the study by Nandenha et al,[18] it was observed that when the potential approaches 0 V, this band is consumed due to the oxidation of these species. ii) ethane, a C2 species reported in oxidative coupling work,[1a,6a] can be identified by the bands observed in 1468 cm^{-1} corresponding to CH_3d-deform of ethane[22] in the hexane fractions (Figure 4c). It rises around 0.2 V, decreases to 0.6 V and disappears by 0.8 V.

Another molecule commonly reported for methane partial oxidation is the formic acid, where the 1102 cm^{-1} band corresponding to C–O stretches[16a] (Figure 4d) appears in all potentials with almost constant intensity. The ethanol, m/z = 46, was observed and identified by CO stretches band at 1044 cm^{-1},[23] appears at −0.1 V and was observed low variation.

The m/z = 44 was attributed to CO_2, acetaldehyde and propane, when observing the FTIR spectra, in hexane solvated samples (Figure 4a) the band at 2883 cm^{-1} corresponding to propane CH_2 stretch + propane CH_3 stretch[24] appears at 0.2 V with decreasing behavior attenuated to 0.6 V and is extinguished at 0.8 V. The band at 1358 cm^{-1} in water sample (Figure 4d) corresponding to acetaldehyde CH_3 s-deform,[25] appears at −0.15 V increase until 0.1 V and disappears. In water samples (Figure 4e) at 650 cm^{-1}, it is possible to see δ_{oop}(OCO) δ(OCO) of CO_2 in solution[26] the signal appears at −0.1 V increase until 0.1 V and the band convolute with other bands.

In a medium where both methanol and formic acid exist, the formation of methyl formate, m/z = 60, is plausible occur between three first potential up to 0.8 V.It was observed by the band at 1757 cm^{-1} related to C=O stretch[27] which intensity showed no relevant variation (Figure 4b). Therefore, the characteristic acetic acid band at 1287 cm^{-1} for OH bend[25] (Figure 4d) appears at 0.2 V and its intensity increases conform the potential increases. In order to better visualize the methane transformation process, scheme 1 shows the reaction pathways detected in this work.

FTIR spectra confirmed the presence of ethane, ethanol, acetaldehyde, acetic acid and propane, C2 and C3 compounds obtained in SER-FC operated with low amount of water in the reaction medium, associated with the use of Pd/C. In scheme 1 presents the reaction steps observed in this work. It is usual for Pd nanoparticles to have some of the PdO phase on the surface;[16a,28] it achieves the ligand effect responsible for lowering the initial C–H bond in methane[12c,13a,14] and water activation.[15] The carbophilic properties of Pd catalyst favors the proximity of the methane and the radicals (scheme 1), as reported by Boyd et al..[9d] The Pd catalyst can starts the propagation of methyl radicals[9d,13a] using less water in the system; the methyl radicals are dimerized to ethane and other present species by the gas-phase coupling reaction as a described by Lim et al..[5]

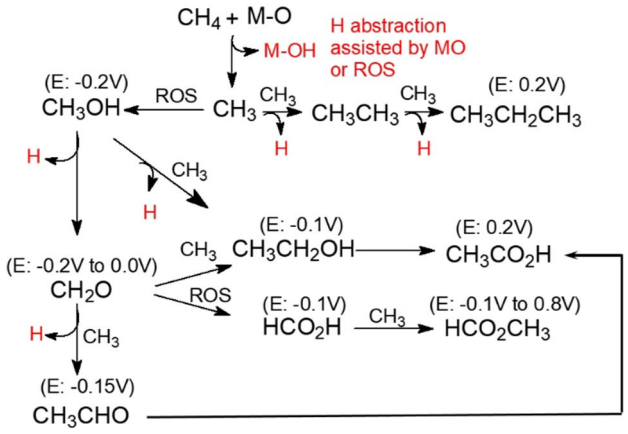

Scheme 1. Parallel path mechanism of methane partial oxidation.

In conclusion, the application of PEM fuel cell as a solid electrolyte reactor is promising for methane valorization by obtaining products with higher added value, such as methanol, formaldehyde and formic acid. Using Pd as an anode catalyst enables to activate water and to lead methyl radicals due to the affinity of Pd with methane.

The operating conditions of the reactor SER-FC allowed the synthesis of other products such as ethanol, ethane, acetic acid, among others. Products C2 and C3, was more easily reported at temperatures much higher in oxidative coupling reactions, however, due to the reduced amount of water compared to other systems, methyl radicals are more likely to collide with carbon-containing molecules, allowing for carbon chain growth.

Finally, further research is necessary to investigate and to develop a method to quantifying the products obtained by DMS.

Acknowledgements

The authors thank the CAPES, FAPESP (2014/09087-4, 2014/50279-4 and 2017/11937-4) and CINE-SHELL (ANP)/FAPESP grants 2017/11937-4 for the fellowships and the financial support this work.

Conflict of Interest

The authors declare no conflict of interest.

Keywords: OCM reaction · methane oxidation · Pd/C · Natural gas to products

[1] a) S. Arndt, T. Otremba, U. Simon, M. Yildiz, H. Schubert, R. Schomäcker, *Appl. Catal. A* **2012**, *425–426*, 53–61; b) Y. Gambo, A. A. Jalil, S. Triwahyono, A. A. Abdulrasheed, *J. Ind. Eng. Chem.* **2018**, *59*, 218–229.
[2] A. B. Sorokin, E. V. Kudrik, L. X. Alvarez, P. Afanasiev, J. M. M. Millet, D. Bouchu, *Catal. Today* **2010**, *157*, 149–154.
[3] B. Wang, S. Albarracín-Suazo, Y. Pagán-Torres, E. Nikolla, *Catal. Today* **2017**, *285*, 147–158.
[4] A. Farsi, S. S. Mansouri, *Arab. J. Chem.* **2016**, *9*, S28-S34.
[5] S. Lim, J.-W. Choi, D. J. Suh, K. H. Song, H. C. Ham, J.-M. Ha, *J. Catal.* **2019**, *375*, 478–492.
[6] a) S. Lim, J.-W. Choi, D. J. Suh, U. Lee, K. H. Song, J.-M. Ha, *Catal. Today* **2019**; b) W. Taifan, J. Baltrusaitis, *Appl. Catal. B* **2016**, *198*, 525–547; c) Z. Luo, D. A. Kriz, R. Miao, C.-H. Kuo, W. Zhong, C. Guild, J. He, B. Willis, Y. Dang, S. L. Suib, P. Nandi, *Appl. Catal. A* **2018**, *554*, 54–63.

[7] a) O. B. Ayodele, *Energ. Convers. Manage.* **2016**, *126*, 537–547; b) L. Arnarson, P. S. Schmidt, M. Pandey, A. Bagger, K. S. Thygesen, I. E. L. Stephens, J. Rossmeisl, *Phys. Chem. Chem. Phys.* **2018**, *20*, 11152–11159.
[8] a) Z. Zakaria, S. K. Kamarudin, *Renewable Sustainable Energy Rev.* **2016**, *65*, 250–261; b) X. Yu, V. De Waele, A. Löfberg, V. Ordomsky, A. Y. Khodakov, *Nat. Commun.* **2019**, *10*, 700; c) A. Hameed, I. M. I. Ismail, M. Aslam, M. A. Gondal, *Appl. Catal. A* **2014**, *470*, 327–335; d) K. Villa, S. Murcia-López, T. Andreu, J. R. Morante, *Appl. Catal. B* **2015**, *163*, 150–155.
[9] a) N. Agarwal, S. J. Freakley, R. U. McVicker, S. M. Althahban, N. Dimitratos, Q. He, D. J. Morgan, R. L. Jenkins, D. J. Willock, S. H. Taylor, C. J. Kiely, G. J. Hutchings, *Science* **2017**, *358*, 223–227; b) J. Jang, K. Shen, C. G. Morales-Guio, *Joule* **2019**, *3*, 2589–2593; c) R. S. Rocha, R. M. Reis, M. R. V. Lanza, R. Bertazzoli, *Electrochim. Acta* **2013**, *87*, 606–610; d) M. J. Boyd, A. A. Latimer, C. F. Dickens, A. C. Nielander, C. Hahn, J. K. Nørskov, D. C. Higgins, T. F. Jaramillo, *ACS Catal.* **2019**, *9*, 7578–7587.
[10] S. Heysiattalab, M. Shakeri, M. Safari, M. M. Keikha, *J. Ind. Eng. Chem.* **2011**, *17*, 727–729.
[11] a) Y. Wang, K. S. Chen, J. Mishler, S. C. Cho, X. C. Adroher, *Appl. Energy* **2011**, *88*, 981–1007; b) G. García, J. A. Silva-Chong, O. Guillén-Villafuerte, J. L. Rodríguez, E. R. González, E. Pastor, *Catal. Today* **2006**, *116*, 415–421; c) F. Alcaide, Ó. Miguel, H.-J. Grande, *Catal. Today* **2006**, *116*, 408–414.
[12] a) B. Lee, T. Hibino, *J. Catal.* **2011**, *279*, 233–240; b) M. Ma, B. J. Jin, P. Li, M. S. Jung, J. I. Kim, Y. Cho, S. Kim, J. H. Moon, J. H. Park, *Adv. Sci.* **2017**, *4*, 1700379; c) M. C. L. Santos, L. C. Nunes, L. M. G. Silva, A. S. Ramos, F. C. Fonseca, R. F. B. de Souza, A. O. Neto, *Chem. Select* **2019**, *4*, 11430–11434.
[13] a) A. Winiwarter, L. Silvioli, S. B. Scott, K. Enemark-Rasmussen, M. Sariç, D. B. Trimarco, P. C. K. Vesborg, P. G. Moses, I. E. L. Stephens, B. Seger, J. Rossmeisl, I. Chorkendorff, *Energ. Env. Sci.* **2019**, *12*, 1055–1067; b) C. Jiménez-Borja, S. Brosda, M. Makri, F. Sapountzi, F. Dorado, J. L. Valverde, C. G. Vayenas, *Solid State Ionics* **2012**, *225*, 376–381; c) Y. He, C. Luan, Y. Fang, X. Feng, X. Peng, G. Yang, N. Tsubaki, *Catal. Today* **2020**, *339*, 48–53.
[14] a) H. Stotz, L. Maier, A. Boubnov, A. T. Gremminger, J. D. Grunwaldt, O. Deutschmann, *J. Catal.* **2019**, *370*, 152–175; b) N. M. Kinnunen, J. T. Hirvi, M. Suvanto, T. A. Pakkanen, *J. Phys. Chem. C* **2011**, *115*, 19197–19202; c) J. F. Weaver, C. Hakanoglu, A. Antony, A. Asthagiri, *Chem. Soc. Rev.* **2014**, *43*, 7536–7547.
[15] a) D. Shi, J. Liu, R. Sun, S. Ji, S. M. Rogers, B. M. Connolly, N. Dimitratos, A. E. H. Wheatley, *Catal. Today* **2018**, *316*, 206–213; b) A. T. N. Nguyen, J. H. Shim, *J. Electroanal. Chem.* **2018**, *827*, 120–127.
[16] a) J. Nandenha, I. Nagahama, J. Yamashita, E. Fontes, J. Ayoub, R. de Souza, F. Fonseca, A. Neto, *Int. J. Electrochem. Sci.* **2019**, *14*, 10819–10834; b) K. Mandal, D. Bhattacharjee, P. S. Roy, S. K. Bhattacharya, S. Dasgupta, *Appl. Catal. A* **2015**, *492*, 100–106; c) F. Munoz, C. Hua, T. Kwong, L. Tran, T. Q. Nguyen, J. L. Haan, *Appl. Catal. B.* **2015**, *174–175*, 323–328; d) Z. Zhang, L. Xin, J. Qi, D. J. Chadderdon, W. Li, *Appl. Catal. B.* **2013**, *136–137*, 29–39.
[17] A. N. Geraldes, D. F. Da Silva, E. S. Pino, J. C. M. Da Silva, R. F. B. De Souza, P. Hammer, E. V. Spinacé, A. O. Neto, M. Linardi, M. C. Dos Santos, *Electrochim. Acta* **2013**, *111*, 455–465.
[18] J. Nandenha, R. M. Piasentin, L. M. G. Silva, E. H. Fontes, A. O. Neto, R. F. B. de Souza, *Ionics* **2019**, *25*, 5077–5082.
[19] E. Tsuchida, Y. Kanada, M. Tsukada, *Chem. Phys. Lett.* **1999**, *311*, 236–240.
[20] M. M. Forde, B. C. Grazia, R. Armstrong, R. L. Jenkins, M. H. A. Rahim, A. F. Carley, N. Dimitratos, J. A. Lopez-Sanchez, S. H. Taylor, N. B. McKeown, G. J. Hutchings, *J. Catal.* **2012**, *290*, 177–185.
[21] K. Z. Gaca-Zając, B. R. Smith, A. Nordon, A. J. Fletcher, K. Johnston, J. Sefcik, *Vib. Spectrosc.* **2018**, *97*, 44–54.
[22] D. W. Lepard, D. E. Shaw, H. L. Welsh, *Can. J. Phys.* **1966**, *44*, 2353–2362.
[23] B. Beden, M. C. Morin, F. Hahn, C. Lamy, *J. Electroanal. Chem. Interfacial Electrochem.* **1987**, *229*, 353–366.
[24] J. N. Gayles, W. T. King, *Spectrochim. Acta* **1965**, *21*, 543–557.
[25] A. O. Neto, J. Nandenha, M. H. M. T. Assumpção, M. Linardi, E. V. Spinacé, R. F. B. De Souza, *Int. J. Hydrogen Energy.* **2013**, *38*, 10585–10591.
[26] J. A. Gómez Castaño, A. Fantoni, R. M. Romano, *J. Mol. Struct.* **2008**, *881*, 68–75.
[27] C.-C. Chuang, W.-C. Wu, M.-C. Huang, I. C. Huang, J.-L. Lin, *J. Catal.* **1999**, *185*, 423–434.
[28] a) C. Xu, Y. Liu, J. Wang, H. Geng, H. Qiu, *J. Power Sources* **2012**, *199*, 124–131; b) W. Du, K. E. Mackenzie, D. F. Milano, N. A. Deskins, D. Su, X. Teng, *ACS Catal.* **2012**, *2*, 287–297.

Manuscript received: February 19, 2020
Revised manuscript received: June 8, 2020
Accepted manuscript online: June 9, 2020
Version of record online: July 14, 2020